Detection of the Farthest Globular Cluster NGC 6715 and Two Other GCs in Gamma-Rays with Fermi-LAT

Min Yuan[1,2], Chongyang Ren[1], Pengfei Zhang[1], Zejun Jiang[1], and Li Zhang[1]

[1] Department of Astronomy, School of Physics and Astronomy, Key Laboratory of Astroparticle Physics of Yunnan Province, Yunnan University, Kunming 650091, China; zhangpengfei@ynu.edu.cn, zjjiang@ynu.edu.cn, lizhang@ynu.edu.cn

[2] School of Mathematics and Statistics, Xianyang Normal University, Xianyang 712000, China

Abstract

In this paper, ∼12 yr long-term Pass 8 data from Fermi Large Area Telescope for the 157 globular clusters are carefully re-analyzed. Besides the 31 globular clusters reported in the fourth Fermi Large Area Telescope catalog Data Release 2, NGC 1851 is identified as a gamma-ray emitter and the significant gamma-ray emissions from NGC 6715 and NGC 6723 are detected. Especially NGC 6715 is located at a distance of 26.8 kpc, so far it is the farthest globular cluster detected in gamma-rays. A detailed analysis for these three globular clusters has been performed, but their gamma-ray pulsation emissions or flux variabilities are not found. The numbers of millisecond pulsars (MSPs) in these globular clusters are estimated under the assumption that each MSP inside globular clusters emits a similar amount of gamma-rays. Some possible origins of gamma-ray emission from globular clusters, such as MSPs, pulsar binary systems and/or dark matter, are discussed.

Key words: (Galaxy:) globular clusters: individual (NGC6715, NGC1851, NGC6723)

1. Introduction

Globular clusters (GCs) are older spherical groups with ages greater than 10^{10} yr. They contain $\sim10^5$ stars within them, the stars hold together by their mutual gravity. In radio and/or optical wavelengths, there are above 150 GCs detected (Harris 1996, 2010 version). Their emissions extend from radio frequencies to GeV energies. On account of high stellar encounter rate in their cores, GCs contain many low-mass X-ray binary systems (LMXBs; Clark 1975; Cheng et al. 1986; Liu et al. 2007). LMXBs are expected to form millisecond pulsars (MSPs; Alpar et al. 1982; Henleywillis et al. 2018; Oh et al. 2020; Zhao et al. 2020). The MSPs can emit gamma-rays through curvature radiation of relativistic electrons/positrons inside their pulsar magnetospheres or through inverse Compton scattering between surrounding soft photons and relativistic electrons/positrons in the pulsar winds of MSPs (Wei et al. 1996; Zhang & Cheng 1997, 2003; Harding et al. 2005; Bednarek & Sitarek 2007; Venter & de Jager 2008; Cheng et al. 2010).

Before 2009, GCs are gamma-ray candidates because they host a large population of MSPs. Thanks to the launch of the Fermi Large Area Telescope (LAT; Atwood et al. 2009), gamma-ray emissions from GCs have been first detected in 47 Tucanae (Abdo et al. 2009, 2010a) and Terzan 5 (Kong et al. 2010). The spectral energy distributions (SEDs) of GCs in gamma-rays show the spectral characteristics of MSPs revealing a hard power-law ($1.0 \lesssim \Gamma \lesssim 2.0$) with exponential cut-offs in the 1–3 GeV energy range (Abdo et al. 2009, 2010a). In NGC 6624, NGC 6626, and NGC 6652, the millisecond gamma-ray pulsations from young MSP PSR J1823−3021A,B1821−24, and J1835−3259B have been detected, respectively (Freire et al. 2011; Johnson et al. 2013; Wu et al. 2013; Zhang et al. 2022). In addition, the majority of MSPs are detected in GCs (Grindlay et al. 2001; Heinke et al. 2005; Abdo et al. 2009, 2010a), for example, 27 MSPs are identified in 47 Tucanae and 39 MSPs are detected in Terzan 5.[3] Especially in Terzan 5, the count of MSPs contains about one-fifth of the total GC pulsar population. Above mentioned cases seem to indicate that gamma-ray emissions of GCs may come from a large population of MSPs that they contain.

Interestingly in 47 Tucanae, a gamma-ray periodic modulation with a period of ∼18.4 hr at a significance level of ∼4.8σ is reported in Zhang et al. (2020). A possible explanation of gamma-rays produced by dark matters (DM) in GCs is also proposed in Abramowski et al. (2011), Feng et al. (2012) and Fortes et al. (2020). This result may shed some light on the gamma-ray origins from GCs.

Based on the above facts, all GCs should have gamma-ray emissions. But in the fourth Fermi Large Area Telescope catalog for Data Release 2 (4FGL-DR2; Abdollahi et al. 2020; Ballet et al. 2020), only about 30 GCs are detected their gamma-rays in ∼GeV (Abdo et al. 2009, 2010a; Kong et al. 2010; Tam et al. 2011b; Eger & Domainko 2012; Zajczyk et al. 2013; Zhou et al. 2015; Tam et al. 2016; Zhang et al. 2016;

---

[3] http://www.naic.edu/~pfreire/GCpsr.html

Table 1
Parameters of Gamma-Ray Globular Clusters

GC Name (1)	Coordinate (2)		Tidal Radius (3)	Position and Error (4)			Offset (5)	Distance (6)
	R.A.	decl.	(arcmin)	R.A.	decl.	Error	(arcmin)	(kpc)
NGC 6715	283.76	−30.48	7.47	283.78	−30.44	± 0.13	2.57	26.8
NGC 1851	78.53	−40.05	11.70	78.49	−40.04	± 0.05	2.00	12.1
NGC 6723	284.89	−36.63	10.51	284.83	−36.56	± 0.26	4.91	8.7

Note. (1) GC identification. (2) Their R.A. (R.A.) and decl. (decl.) as listed in Harris (1996, and 2010 version) in J2000. (3) Tidal radius for three GCs. (4) Best-fit positions and their errors of results derived by *gtfindsrc*. (5) The offsets from their coordinates (1). (6) Distances from the Sun as listed in Harris (1996, and 2010 version).

Lloyd et al. 2018; de Menezes et al. 2019; MAGIC Collaboration et al. 2019; Ndiyavala et al. 2019; Ballet et al. 2020; Song et al. 2021; Wu et al. 2022; Yuan et al. 2022). Motivated by data accumulation of Fermi-LAT, improving gamma-ray background models, and enlargement of the gamma-ray GCs sample, the gamma-ray events gathered by Fermi-LAT observations from 157 GCs are re-analyzed to search for new gamma-ray emitters here.

In this work, three point-like gamma-ray sources that are spatially consistent with NGC 6715, NGC 1851, and NGC 6723 are reported. It may be concluded that GC NGC 1851 is a gamma-ray emitter with post-trial significance $>7\sigma$, and other two GCs are possible gamma-ray emitters with post-trial significance $\sim4\sigma$. Some historical information for these GCs is shown in Table 1. Based on the previous literature, the most of GCs detected in gamma-rays are those within the distances of only a several kilo-parsecs (kpc) from the Sun (Abdo et al. 2009, 2010a; Kong et al. 2010; Tam et al. 2011b; Zhou et al. 2015; Zhang et al. 2016). While NGC 6715 is located at a distance of 26.8 kpc, so far it is the farthest globular cluster in gamma-rays. This paper is organized as follows: In Section 2, the reduction for the Fermi-LAT observations is described, the main results are shown in Section 3. In Section 4, a summary and some discussion are given. The uncertainties given in this work are only 1σ statistical errors.

2. Data Analysis and Results

In our data reduction, Fermi-LAT Pass 8 events with energy bands of 0.1–500 GeV are selected, which cover the period from 2008 August 8 to 2020 December 29 (i.e., MJD: 54,686 −59,212). The events within a $20° \times 20°$ region of interest (ROI) centered at the coordinates listed in Harris (1996, and 2010 version) are selected, and the same coordinates are used in the following analysis. The *FRONT+BACK* SOURCE class photon-like events (evclass = 128 and evtype = 3) are used in the analysis. The events with zenith angles $>90°$ are excluded, only high-quality data with DATA_QUAL > 0 and LAT_ CONFIG == 1 in the good time intervals are kept, instrumental response function "P8R3_SOURCE_V3" is adopted. The exposure maps are calculated with tool *gtexpcube2* to account

for contributions from the sources. The sources outside the ROI also affect the data analysis for sources in the ROI because of large PSF of Fermi-LAT at low energies. As recommend by Fermi-LAT Collaboration, the exposure maps of $60° \times 60°$ region are created to compensate contributions from sources outside the ROI. Two files, gll_iem_v07.fits and iso_ P8R3_SOURCE_V3_v1.txt, are used to model the gamma-ray diffuse emissions from the two backgrounds (the diffuse gamma-rays from Galactic and extragalactic). In the data analysis, the Fermitools-2.0.0 package[4] is used.

For each target, a model file is created with a script make4FGLxml.py based on 4FGL-DR2.[5] The model file is composed of the known 4FGL-DR2 sources (Abdollahi et al. 2020; Ballet et al. 2020). 4FGL-DR2 has the largest population of gamma-ray sources based on 10 yr data with test statistic (TS) > 25. For the model file, it includes point-like and spatial extended sources. Especially for the latter we fit them with spatial diffuse templates updated by 4FGL-DR2. In the model file the parameters of flux normalizations and the spectral shapes of all sources within $5°$ are set free, the normalizations for the sources within $5°$–$10°$ are free and their parameters of the spectral shapes are fixed at the values in 4FGL-DR2 catalog, the parameters of other sources in the model file beyond $10°$ are fixed to the values at 4FGL-DR2 catalog, and only the significantly variable sources (i.e., *Variablility_Index* $\geqslant 72.44$), their normalizations are set free. The data are divided into 37 equal logarithmically spaced bins in energy dimensionality with a spatial pixel size of $0°.1 \times 0°.1$ (i.e., 200×200 pixel^2). Then a binned maximum likelihood analysis is performed between the entire data and the model file. The tool *gtlike* is employed to derive the best-fit parameters (flux, spectral index, and TS value), and they are saved as a model file (Model$_0$).

Basing on Model$_0$, a residual TS map is created by employing the tool *gttsmap*, *gttsmap* calculates the TS value for each grid of locations on sky by removing the sources within the model file in order to highlight the weaker sources. In the residual TS map, for the brightest gamma-ray excess

---

4   https://github.com/fermi-lat/Fermitools-conda/
5   https://fermi.gsfc.nasa.gov/ssc/data/analysis/user/

Table 2
Results for the Three GCs

GC Name	Spectral Model	Post-trial Significance (σ)	Photon Index γ (E_{cut} GeV)	Photon Flux (1) (10^{-9} cm^{-2} s^{-1})	Energy Flux (2) (10^{-12} erg cm^{-2} s^{-1})	Luminosity (3) (10^{34} erg s^{-1})	N_{MSP} (4)	$\mathcal{N}_{\mathrm{MSP}}$ (5)
NGC 6715	PL	4.0	2.55 ± 0.19	5.89 ± 1.20	2.64 ± 0.54	22.60 ± 4.62	157 ± 69	none
	PLE	4.0	1.84 ± 1.25 (3.00 ± 1.41)	3.09 ± 1.89	1.88 ± 0.39	16.10 ± 3.34	112 ± 49	
NGC 1851	PL	7.6	2.50 ± 0.11	4.54 ± 0.63	2.14 ± 0.30	3.74 ± 0.52	26 ± 11	14
	PLE	7.7	2.00 ± 0.35 (3.89 ± 1.39)	3.00 ± 0.45	1.66 ± 0.23	2.90 ± 0.40	20 ± 8	
NGC 6723	PL	3.6	2.24 ± 0.12	2.96 ± 0.67	2.13 ± 0.48	1.92 ± 0.43	13 ± 6	none
	PLE	4.2	1.51 ± 0.35 (3.00 ± 1.25)	1.78 ± 0.97	1.53 ± 0.33	1.38 ± 0.30	10 ± 4	

Notes. (1) Integrated photon flux in units of 10^{-9} cm^{-2} s^{-1} in energy range of 0.1–500 GeV. (2) Integrated energy flux in units of 10^{-12} erg cm^{-2} s^{-1} in energy range of 0.1–500 GeV. (3) Luminosity in units of 10^{34} erg s^{-1} in energy range of 0.1–500 GeV. (4) Evaluated number of MSPs (N_{MSP}), where their errors were calculated with the error propagation formula of luminosities. (5) Detected number of MSPs ($\mathcal{N}_{\mathrm{MSP}}$).

having a point source distribution, we derive its position by employing the tool *gtfindsrc*. And a point source with a spectral shape of a single power law (PowerLaw) is added at the position in the Model$_0$. We re-run the likelihood analysis, obtain another model file (Model$_1$), and create a new residual TS map. This procedure is repeated until no obvious gamma-ray excesses with TS > 16. And the best-fit parameters are saved as a final best-fit model file (Model$_f$). If there is a gamma-ray excess with the point source distribution and having TS > 25 within the tidal radii of one GC, it becomes a candidate for a new gamma-ray GC. Then we carry out a further analysis basing on Model$_f$. Their tidal radii are available on the Internet[6] (Harris 1996, 2010 version).

For the GC candidates, two spectral shapes are used to fit their events in the data analysis. The spectral model of PowerLaw with the formula of $\frac{dN}{dE} = K\left(\frac{E}{E_0}\right)^{-\gamma}$ is first employed, where parameters K and γ are the normalization (gamma-ray flux density) and energy spectral slope respectively. Because of a large population of MSPs within GCs, their gamma-ray spectra have a similar shape to those found in pulsars in gamma-ray bands. A subexponential cut-off power law (PLSuperExpCutoff) with the formula of $\frac{dN}{dE} = K\left(\frac{E}{E_0}\right)^{-\gamma_1} \exp(-\left(\frac{E}{E_c}\right)^b)$ is also used to fit events from the GC candidates, where γ_1, b, and E_c represent low-energy spectral slope, exponential index and cutoff energy, respectively. Since three GCs are relative weaker in gamma-ray comparing with sources in 4FGL-DR2. Their population of events is too small to restrict the parameters for PLSuperExpCutoff model. We fix b at the value of 1.0 adopted in Abdo et al. (2010a) and list the best-fit parameters in Table 2.

In this work, the data from 157 GCs are re-analyzed. Besides the 31 GCs reported in 4FGL-DR2 by Abdollahi et al. (2020) and Ballet et al. (2020), gamma-rays from these three point-like

gamma-ray excesses are found, which are spatially consistent with NGC 6715, NGC 1851, and NGC 6723. Their best-fit results are shown in Table 2. They have higher TS values (over 25). Based on the aforementioned procedure, six and three point sources are added in the model files for NGC 6715 and NGC 6723 in a $5° \times 5°$ region, respectively. Following the previous literature, three TS maps with a $5° \times 5°$ region and spatial pixel size of $0°.1 \times 0°.1$ are created for the three GCs by removing the target in the Model$_f$. Then we calculate the significance for each GC based on the chi-square distribution. In our analysis, we tried to search gamma-rays from 126 (=157 − 31) GCs; therefore, our trial number is 126. After accounting for this trial factor, the post-trial detection significances are derived and listed in Table 2. The three TS maps without smoothing are shown in Figure 1, and the color bar represent TS value scaled with color. The results of other gamma-ray GCs in 10 yr 4FGL-DR2 in our analysis are listed in Table 3.

In order to examine the SED properties of the three GCs in gamma-rays, the data are also divided into logarithmically equal bins in energy dimensionality. In this step, all spectral parameters are fixed but the normalization is free for the Model$_f$. The fluxes for each energy bin in energy range from 100 MeV to 500 GeV are obtained by employing tool *gtlike*, and their SEDs are showed in Figure 2. Three GCs are weaker sources in gamma-rays compared to sources listed in 4FGL-DR2. Their spectra do not show the shape as the most significantly detected GCs, e.g., 47 Tucanae (Abdo et al. 2009, 2010a) or Terzan 5 (Kong et al. 2010). The similar spectra are also shown in Tam et al. (2011b), Zhou et al. (2015), and Zhang et al. (2016).

The light curves with time bin of 180 days (half a year) for these three GCs are also obtained to examine their possible variability in the gamma-ray flux (based on the model in deriving their SEDs). For each time bin, the light curves are derived by employing the unbinned maximum likelihood fitting technique. The light curve for each GC is fitted with a constant
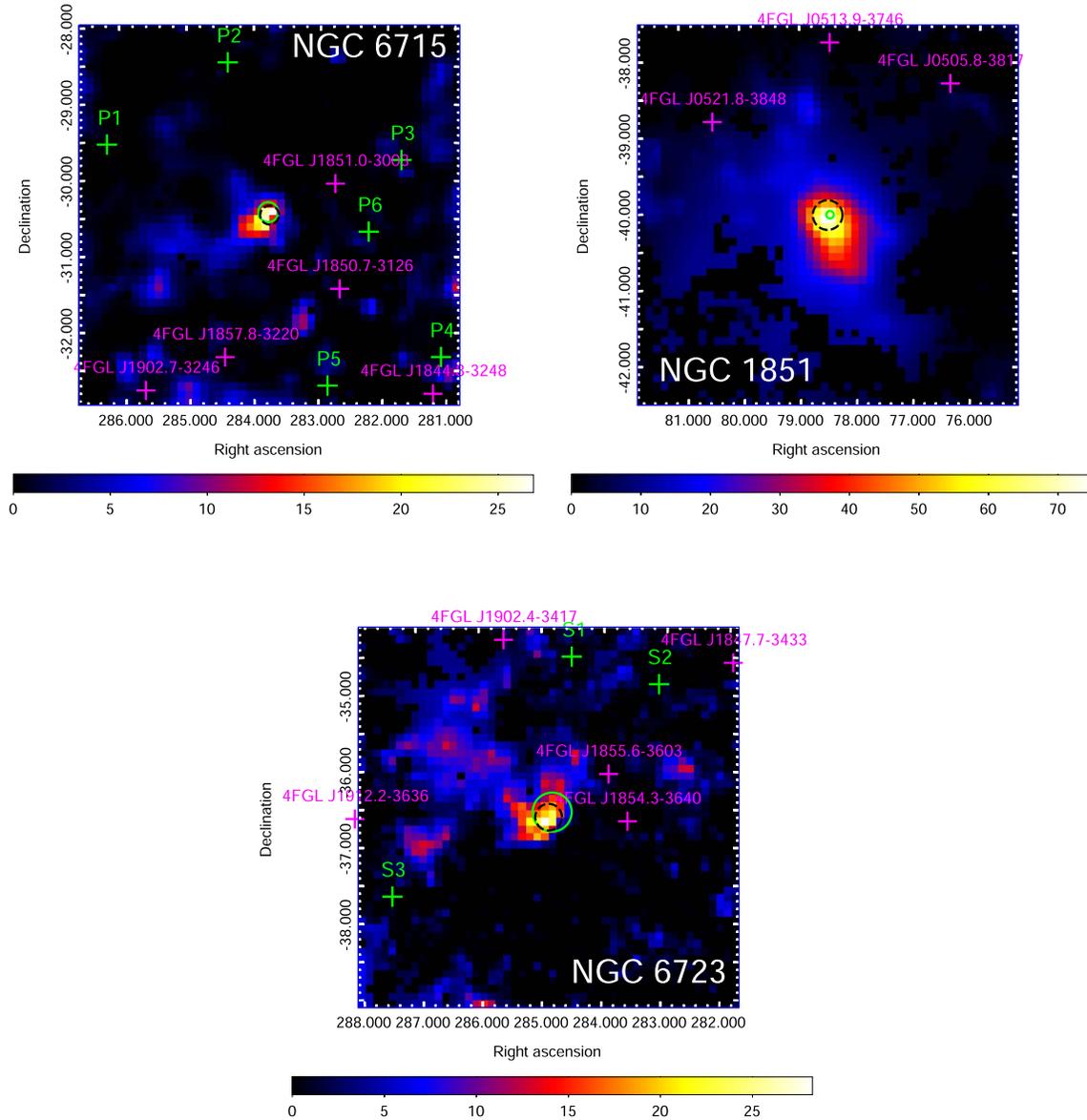
[6] https://physwww.mcmaster.ca/~harris/Databases.html

Figure 1. TS maps of $5° \times 5°$ region with a spatial pixel size of $0°.1 \times 0°.1$ for NGC 6715, NGC 1851, and NGC 6723 with events selected over 100 MeV. The color bars represent TS values scaled with color. The black dashed circles stand for their tidal radii centered coordinates as listed in Harris (1996, and 2010 version). The green solid circles stand for the best-fit centroids of the gamma-ray emission with 1σ statistical errors indicating their radii. The purple crosses are gamma-ray sources reported in 4FGL-DR2 within $5° \times 5°$ region.

using a χ^2 minimization procedure, and no significant variability is detected at confidence level of 3σ.

For NGC 1851, its possible gamma-ray pulsation from individual pulsar contained within itself is also studied with the routine TEMPO2[7] using the ephemerides provided by Manchester et al. (2005), Nan et al. (2011), Booth & Jonas (2012), Li & Pan (2016), Ridolfi et al. (2019). No significant

detection is found. For NGC 6715 and NGC 6723 there is no radio pulsar detected within them so far.

3. Results of the Three GCs

3.1. Gamma-Ray GCs

The best-fit results of our analysis for the gamma-ray GCs listed in 10 yr 4FGL-DR2 (Abdollahi et al. 2020; Ballet et al. 2020) are shown in Table 3. The topic of our work is the new

---

[7] http://tempo.sourceforge.net/

4

Table 3
Results of the GCs Reported in 4FGL-DR2

GC Name	TS	Photon Index Index1 Index2	Photon Flux (1) $(10^{-9}\ \mathrm{cm}^{-2}\ \mathrm{s}^{-1})$	Energy Flux (2) $(10^{-12}\ \mathrm{erg}\ \mathrm{cm}^{-2}\ \mathrm{s}^{-1})$	Luminosity (3) $(10^{34}\ \mathrm{erg}\ \mathrm{s}^{-1})$	N_{MSP} (4)	$\mathcal{N}_{\mathrm{MSP}}$ (5)	Distance (kpc)
		$\alpha\ \beta$ (LP)						
47 Tuc	8324.1	$1.78 \pm 0.02\ 0.33 \pm 0.02$	14.53 ± 0.28	17.76 ± 0.35	4.29 ± 0.08	29 ± 12	27	4.5
Terzan5	6150.8	$2.22 \pm 0.01\ 0.25 \pm 0.01$	87.66 ± 1.52	80.49 ± 1.39	45.68 ± 0.79	317 ± 123	39	6.9
Omega Cen	1093.4	$2.26 \pm 0.07\ 0.54 \pm 0.07$	5.87 ± 0.27	8.43 ± 0.39	2.72 ± 0.13	19 ± 7	5	5.2
NGC 6388	1547.4	$2.09 \pm 0.01\ 0.31 \pm 0.01$	16.85 ± 0.57	16.49 ± 0.56	19.27 ± 0.65	134 ± 52	None	9.9
M62	1564.7	$1.99 \pm 0.03\ 0.36 \pm 0.02$	14.88 ± 0.51	17.21 ± 0.59	9.49 ± 0.33	66 ± 26	7	6.8
NGC 6440	387.9	$2.37 \pm 0.06\ 0.24 \pm 0.01$	16.90 ± 1.12	13.89 ± 0.92	11.96 ± 0.79	83 ± 33	8	8.5
NGC 6652	192.4	$2.25 \pm 0.10\ 0.35 \pm 0.08$	4.66 ± 0.40	4.36 ± 0.38	5.20 ± 0.45	36 ± 14	2	10.0
NGC 6752	254.8	$1.91 \pm 0.11\ 0.73 \pm 0.10$	1.62 ± 0.13	2.27 ± 0.18	0.43 ± 0.03	3 ± 1	9	4.0
M80	134.7	$2.37 \pm 0.10\ 0.05 \pm 0.06$	9.29 ± 0.98	5.66 ± 0.59	6.75 ± 0.70	47 ± 19	None	10.0
NGC 6541	176.2	$2.14 \pm 0.12\ 0.29 \pm 0.09$	4.85 ± 0.43	4.04 ± 0.36	2.71 ± 0.24	19 ± 8	None	7.5
NGC 6717	115.3	$2.02 \pm 0.16\ 0.47 \pm 0.13$	1.20 ± 0.23	3.04 ± 0.35	1.83 ± 0.21	13 ± 5	None	7.1
NGC 6441	719.4	$2.15 \pm 0.03\ 0.29 \pm 0.01$	15.27 ± 0.72	13.58 ± 0.64	21.78 ± 1.03	151 ± 59	7	11.6
NGC 6316	407.0	$2.32 \pm 0.04\ 0.21 \pm 0.01$	15.89 ± 0.93	12.29 ± 0.72	15.85 ± 0.93	110 ± 43	None	10.4
NGC 6218	38.8	$1.53 \pm 0.49\ 1.20 \pm 0.57$	0.16 ± 0.03	0.94 ± 0.20	0.26 ± 0.05	2 ± 1	1	4.8
NGC 6304	44.4	$2.13 \pm 0.41\ 0.52 \pm 0.01$	1.73 ± 0.29	2.53 ± 0.42	1.05 ± 0.17	7 ± 3	None	5.9
Terzan 2	76.0	$2.12 \pm 0.62\ 0.16 \pm 0.01$	5.25 ± 0.70	6.39 ± 0.85	4.28 ± 0.57	30 ± 12	None	7.5
Terzan 1	110.4	$1.47 \pm 0.11\ 2.14 \pm 0.01$	1.18 ± 0.01	5.38 ± 0.03	2.88 ± 0.02	20 ± 8	7	6.7
NGC 6402	82.3	$2.18 \pm 0.17\ 0.37 \pm 0.13$	3.22 ± 0.41	3.32 ± 0.42	3.42 ± 0.43	24 ± 10	5	9.3
GLIMPSE02	190.1	$2.53 \pm 0.08\ 0.27 \pm 0.01$	27.85 ± 2.46	21.41 ± 1.89	7.72 ± 0.68	54 ± 21	None	5.5
GLIMPSE01	806.6	$2.37 \pm 0.05\ 0.34 \pm 0.04$	35.38 ± 1.74	43.09 ± 2.12	9.06 ± 0.45	63 ± 25	None	4.2
NGC 6838	56.7	$2.64 \pm 0.39\ 0.01 \pm 0.10$	11.48 ± 1.71	4.67 ± 0.69	0.89 ± 0.13	6 ± 3	4	4.0
		$\gamma_1\ b$ (PLE2)						
NGC 6624	937.1	$1.22 \pm 0.03\ 0.65 \pm 0.01$ a: 9.15 ± 0.16	11.43 ± 0.51	12.29 ± 0.55	9.14 ± 0.41	63 ± 25	10	7.9
		γ (PL)						
NGC 1904	26.7	2.25 ± 0.36	1.98 ± 0.50	1.39 ± 0.35	2.76 ± 0.69	19 ± 9	None	12.9
NGC 6341	68.8	2.54 ± 0.13	4.53 ± 0.65	2.06 ± 0.29	1.69 ± 0.24	12 ± 5	1	8.3
NGC 2808	239.1	2.71 ± 0.09	13.67 ± 1.01	5.24 ± 0.39	5.76 ± 0.43	40 ± 16	None	9.6
NGC 362	27.4	2.15 ± 0.18	1.09 ± 0.26	0.95 ± 0.23	0.84 ± 0.20	6 ± 3	None	8.6
NGC 5904	40.7	2.21 ± 0.13	2.75 ± 0.52	2.12 ± 0.40	1.42 ± 0.27	10 ± 4	7	7.5
NGC 6139	125.0	2.46 ± 0.08	15.67 ± 1.59	7.78 ± 0.79	9.46 ± 0.96	66 ± 26	None	10.1
NGC 6397	70.1	2.73 ± 0.55	9.77 ± 1.54	3.69 ± 0.58	0.23 ± 0.04	2 ± 1	2	2.3
2MS-GC01	260.0	2.57 ± 0.06	78.37 ± 7.70	34.37 ± 3.38	5.31 ± 0.52	37 ± 15	None	3.6
NGC 7078	126.4	2.76 ± 0.09	12.54 ± 1.25	4.64 ± 0.46	5.98 ± 0.59	42 ± 17	9	10.4

Note. Same as Table 2. But the models of LP and PLE2 mean LogParabola and PLSuperExpCutoff2 with the formulas of $\frac{dN}{dE} = N_0 \left(\frac{E}{E_b}\right)^{-(\alpha + \beta \log(E/E_b))}$ and $\frac{dN}{dE} = N_0 \left(\frac{E}{E_0}\right)^{-\gamma_1} \exp(-aE^b)$, they have same spectral shapes as that reported in 10 yr 4FGL-DR2 (Abdollahi et al. 2020; Ballet et al. 2020).

detections of gamma-ray GCs, and we ignore the results of non-detection ones. The following information are about the three significantly detected GCs.

3.1.1. NGC 6715

NGC 6715 (also known as Messier 54 or M54) is a GC hosting about 1 million stars. It is one of the most compact globular cluster known and is located at the constellation Sagittarius. It has been proposed that NGC 6715 has an intermediate mass black hole of $\sim 9400\ M_\odot$ in its center (Ibata et al. 2009). At the radio band, there is no pulsar detected in this cluster. In the gamma-ray band, its events above 100 MeV are fitted with two energy spectral models, and the similar TS values of ~ 29 are obtained, which is translated to 5.4σ. After accounting for the trial factor, its post-trial detection significance value is $\sim 4.0\sigma$. NGC 6715 is identified as a possible gamma-ray emitter. Until now, this cluster is the farthest GC detected with gamma-ray emission with a distance of 26.8 kpc away from the Sun. Its nominal position is R.A. $= 283°.76$ and decl. $= -30°.48$, and our best-fit position is R.A. $= 283°.78$ and decl. $= -30°.44$ (with an error of $0°.13$). The gamma-ray derived position is well within the tidal radius of NGC 6715 ($7'.47$) with an offset of $2'.57$. Its gamma-ray luminosities in two spectral models are $L^{\mathrm{PL}}_{0.1-500\,\mathrm{GeV}} = (22.60 \pm 4.62) \times 10^{34}$ erg s^{-1} and $L^{\mathrm{PLE}}_{0.1-500\,\mathrm{GeV}} = (16.10 \pm 3.34) \times$
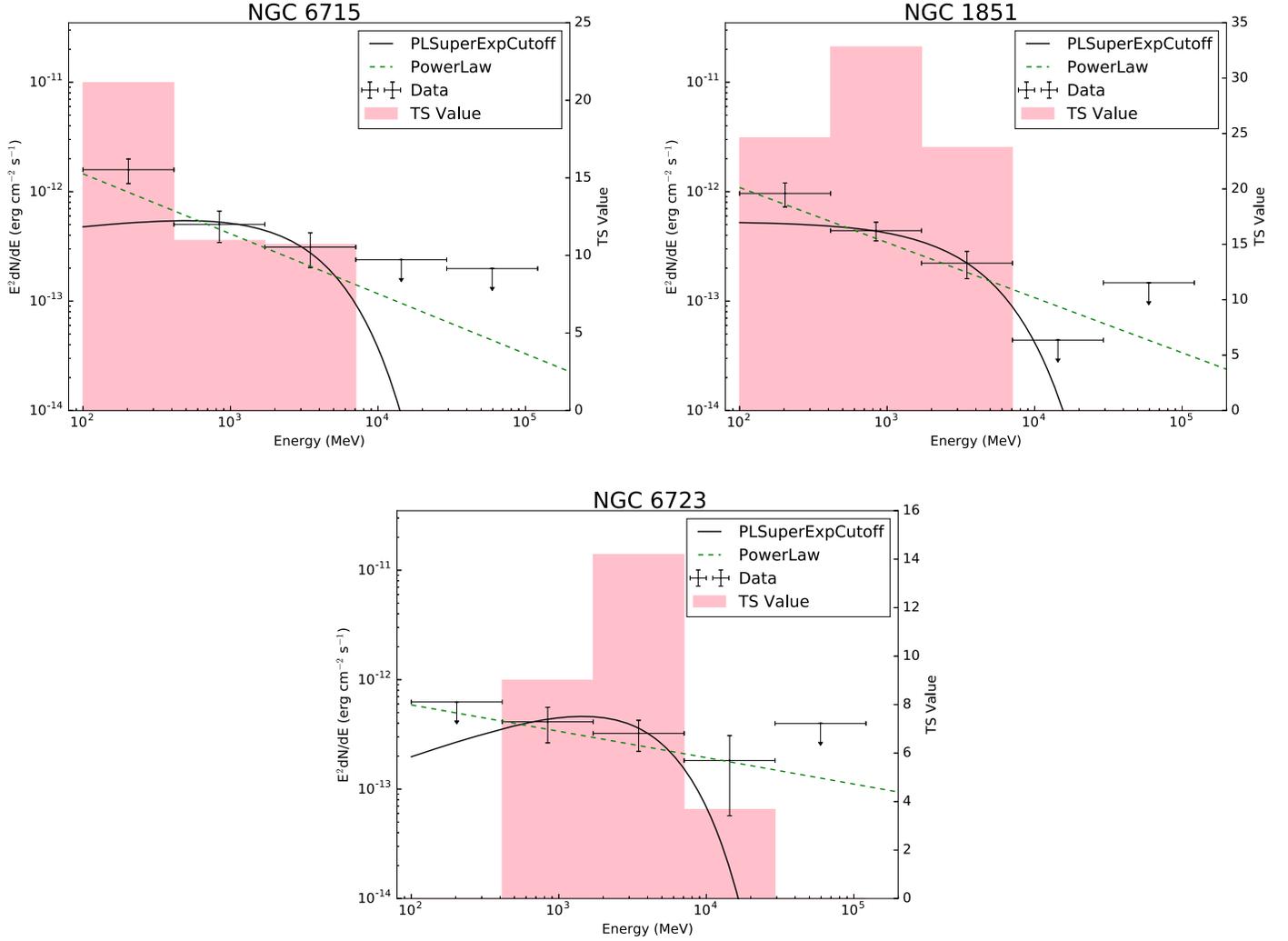
Figure 2. Spectral energy distributions for NGC 6715, NGC 1851, and NGC 6723. The green dashed lines indicate the best-fit models with spectral function of PowerLaw, and the black solid lines represent the best-fit models with spectral function of PLSuperExpCutoff. We also show the TS values for each data point with pink bars. The detailed information of best-fit model spectral parameters is listed in Table 2.

10^{34} erg s^{-1}, respectively. The observed gamma-ray luminosities imply about 130 radio pulsars hosted in NGC 6715. The other detailed information of best-fit for NGC 6715 is listed in Table 2. Its residual TS map and SED above 100 MeV are shown in the upper right panel of Figures 1 and 2, respectively. We added six point sources named P1−6 in the creating of TS map to show NGC 6715 obviously. Their positions of R.A. and decl. correspond to 286°.22 and −29°.53, 284°.39 and −28°.47, 281°.77 and −29°.74, 281°.10 and −32°.32, 282°.86 and −32°.72, 282°.25 and −30°.69, respectively. We marked them with green crosses shown in the upper left panel of Figure 1.

3.1.2. NGC 1851

NGC 1851 has the highest TS and is most significantly detected here. It is located at a distance of 12.1 kpc from the Sun. Until now, in total of 14 MSPs (PSR J0514−4002A−N)

are found in this GC with spin periods of several milliseconds. Their spin periods span from approximately 2.8 ms up to 32.7 ms detected in radio bands (Nan et al. 2011; Ridolfi et al. 2019). Seven of them (PSR J0514−4002A, E, F, G, H, I, L) are found in pulsar binary systems. Especially, MSP J0514−4002A is proposed in a neutron star binary system with a long orbital period of 18.79 days (Ridolfi et al. 2019). The other six orbital periods of pulsar binaries are not detected until now. In the gamma-ray band, the events with energy range of 0.1–500 GeV for NGC 1851 are selected here, the PowerLaw and the PLSuperExpCutoff spectral models are used to fit the events respectively, the best-fit photon spectral indexes and other detailed information are obtained, see in Table 2. Based on both spectral models, the TS values of ∼72 and 74 are obtained, which corresponds to a detection significance of 8.5σ, the post-trial significance is 7.7σ. Therefore, NGC 1851 would

be a gamma-ray emitter. Its gamma-ray best-fit position extracted by *gtfindsrc* is R.A. $= 78°53$ and decl. $= 40°05$ (J2000) with 1σ error of $0°05$, which falls well within the nominal position (R.A. $= 78°49$ and decl. $= 40°04$) with a tidal radius of $11′70$, the offset between two positions is $2′0$. The number of MSPs contained within NGC 1851 may be ~20 (listed in Table 2). It is more than the number of MSPs detected in NGC 1851. Its residual TS map above 100 MeV is shown in the upper left panel of Figure 1. NGC 1851 has clear background in the gamma-ray band. Only three gamma-ray sources in 4FGL-DR2 are detected within $5° \times 5°$ region, the separation between NGC 1851 and the closest source 4FGL-DR2 J0521.8-3848 is $\sim2°$. The SED of NGC 1851 is shown in the upper left panel of Figure 2.

3.1.3. NGC 6723

NGC 6723 is about 12.5 billion years old, located at a moderate distance of 8.7 kpc away from the Sun in the constellation Sagittarius. Although many physical properties of NGC 6723 has been studied in the past, it still remains poorly understandings in many wave bands. In the radio band, there is no pulsar detected within it. Its gamma-ray emission is also not reported by Abdollahi et al. (2020), Ballet et al. (2020). Here, the events over 100 MeV around the position of NGC 6723 are selected and fitted with two spectral models. TS values of 25 for PowerLaw and 31 for PLSuperExpCutoff are obtained. This cluster may be a possible gamma-ray emitter considering for trial factor. Its gamma-ray best-fit position is derived at R.A. $= 284°83$ and decl. $= -36°56$ with an error of $0°26$, which is offset by $4′91$ from its nominal position of R.A. $= 284°89$ and decl. $= -36°63$. Its tidal radius is $10′51$. The derived gamma-ray position is well within the tidal radius circle centered at its nominal position. The gamma-ray luminosities are $L_{0.1-500\,\text{GeV}}^{\text{PL}} = (1.92 \pm 0.43) \times 10^{34}$ erg s^{-1} for Power-Law model and $L_{0.1-500\,\text{GeV}}^{\text{PLE}} = (1.38 \pm 0.30) \times 10^{34}$ erg s^{-1} for PLSuperExpCutoff. Based on its gamma-ray luminosities, the number of MSPs contained within NGC 6723 estimated to be ~10. Other best-fit results are listed in Table 2. The residual TS map and SED are shown in the lower left panel of Figures 1 and 2. We added three point sources named S1−3 in the creating NGC 6723's TS map. Their positions of R.A. and decl. are $284°52$ and $-34°52$, $283°12$ and $-34°87$, $287°48$ and $-37°65$, respectively. We marked them with green crosses shown in the lower panel of Figure 1.

3.2. Estimated Numbers of MSPs

In general, GCs emit gamma-rays because they contain large populations of MSPs. The number of MSPs in these clusters can be estimated by taking the average spin-down power with a value of $\langle \dot{E} \rangle = (1.8 \pm 0.7) \times 10^{34}$ erg s^{-1} and presuming each MSP presented in GCs emitting similar amount of gamma-rays (Abdo et al. 2009). The total number of MSPs is

evaluated by $N_{\text{MSP}} = L_\gamma / \langle \dot{E} \rangle \langle \eta_\gamma \rangle$, where N_{MSP}, L_γ, $\langle \dot{E} \rangle$, and $\langle \eta_\gamma \rangle$ are the number of MSPs, the isotropic gamma-ray luminosity of each cluster, the average spin-down power for each MSP, and the estimated average spin-down to gamma-ray luminosity conversion efficiency respectively. For the three GCs, $\langle \eta_\gamma \rangle$ value of 0.08 is adopted. The isotropic gamma-ray luminosities of these clusters are obtained with $L_\gamma = 4\pi S d^2$, where S and d are the observed energy flux and the distance from the Sun to the GCs. The observed energy fluxes and the estimated numbers of MSPs for each GC are summarized in Tables 2 and 3. These estimated numbers are much higher than the counts of MSPs identified in the radio and/or X-ray observations. Especially in GC NGC 6715, the estimated number is ~130, but no pulsar is detected in it up to now.

It is commonly believed that the number of LMXBs in GCs is correlated with their stellar encounter rates (Gendre et al. 2003). We know that the MSPs are the progeny of LMXBs (Alpar et al. 1982). A positive correlation between the estimated number of MSPs and the stellar encounter rates (Γ_c) for GCs are shown in Abdo et al. (2009). The stellar encounter rates are derived with $\Gamma_e = \rho_0^{1.5} r_c^2$, ρ_0 is estimated with $\rho_0^{\text{Harris}} d^{\text{Harris}} / d$ (Djorgovski 1993) and $r_c = d \tan\theta_c$, where ρ_0^{Harris}, d^{Harris}, d, r_c and θ_c are the central cluster density in Harris 2003 revision, the distances in Harris 2003 revision, the distances, the cluster core radius in units of pc and the cluster core radius in units of radian. For M62 (NGC 6266), its stellar encounter rate is Γ_e is 6.547×10^6 $L_\odot^{1.5}$ pc$^{-2.5}$ with $\rho_0^{\text{Harris}} = 10^{5.14}$ $L_\odot$ pc^{-3}, $d^{\text{Harris}} = 6.9$ kpc, $d = 6.6$ kpc, and $\theta_c = 0′18$, then Γ_e is normalized to value of 100 (Abdo et al. 2009). The same calculation is adopted for GC's stellar encounter rates as Abdo et al. (2009). Using the gamma-ray results listed in Tables 2 and 3, the relationships attached between other intrinsic characteristics of GCs are shown in Figure 3, as shown in Hui et al. (2011), the parameter values aforesaid are obtained from the Harris 2010 revision.[8] We show the plots of the gamma-ray luminosity versus stellar encounter rate (Γ_e) and metallicity [Fe/H] for GCs in Figure 3.

The correlations of N_{MSPs} versus [Fe/H] and N_{MSPs} versus Γ_e are fitted by a linear regression with a least squares minimization procedure.[9] Their best-fit results are given by $\log_{10}(N_{\text{MSPs}}) = (0.40 \pm 0.16) \times$ [Fe/H] $+ (1.88 \pm 0.20)$ and $\log_{10}(N_{\text{MSPs}}) = (0.29 \pm 0.10) \times \log_{10}(\Gamma_e) + (1.11 \pm 0.14)$, respectively.

4. Summary and Discussion

Based on the ~12 yr long-term Pass 8 data from Fermi-LAT, 157 GCs have been systematically analyzed in this paper. Besides 31 GCs that have been reported in previous works (Abdo et al. 2009, 2010a, 2010b; Kong et al. 2010; Tam et al.
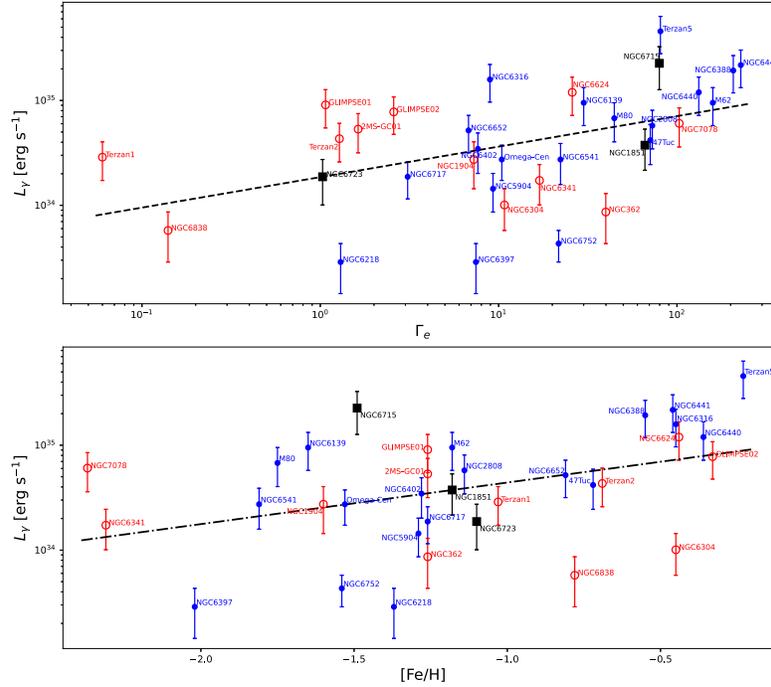

Figure 3. (Top) Gamma-ray luminosity vs. stellar encounter rate (Γ_e) for GCs. (Bottom) Gamma-ray luminosity vs. metallicity [Fe/H] for GCs. The GCs reported in the previous literature are marked with blue circles, the GCs increased in 10 yr 4FGL-DR2 are marked with red circles, the three GCs reported here are marked with black squares.

2011b; Nolan et al. 2012; Acero et al. 2015; Zhou et al. 2015; Zhang et al. 2016; Lloyd et al. 2018; de Menezes et al. 2019; Abdollahi et al. 2020), our results show that three GCs are detected with significant gamma-ray emissions, they are NGC 6715, NGC 1851, and NGC 6723. From our analysis, main results are as follows. First, GC NGC 1851 is a gamma-ray emitter with TS $\sim$72 (having post-trial $>7\sigma$), NGC 6715 and NGC 6723 are possible gamma-ray emitters with TS $>$ 25 (having post-trial $\sim4\sigma$). Second, besides 14 radio pulsars detected in NGC 1851, no pulsar is found in NGC 6715 and NGC 6723. Finally, NGC 6715 is the most distant at a distance of 26.8 kpc. Moreover, NGC 6715 is the most furthest GC in which gamma-rays are detected, its distance is much further than other GCs' reported by previous works, their distances are listed in Table 3. Some point sources are added in the creating of TS maps for NGC 6715 and NGC 6723 to show them obviously. From the TS maps in the Figure 1, there is no obvious gamma-ray source near by the three GCs. To check for possible structures in the GCs, we also created the residual TS maps by removing all sources in the final model file, but only one point source at the position for each GC. No obvious gamma-ray source is shown in their residual TS maps. So the gamma-ray excess corresponding to each GC is well described with a point source.

In our data analysis, we also calculated their TS maps for the non-detections GCs in gamma-ray. Despite some of them has higher TS values ($>$25), while their TS maps have

large spatial extension in $5° \times 5°$ ROI at several hundred MeV, rather than a point-like distribution. Moreover their positions of the strongest gamma-ray emission are located at outside of their tidal radii. We do not take them as our detections here.

To exclude possibility that gamma-rays from AGNs behind three GCs, we examine all sources listed in simbad[10] within $3°$ centered at positions listed in Table 1 for the three GCs. For NGC 6715, we find a nearest AGN ([WGH2011] VLA J185510.68-302650.9) with a distance of $0°.04$ away from it, the offset is a little bit larger for Fermi-LAT. The AGN is not classified as Blazar, Seyfert 1 galaxy or radio galaxy, the probability of gamma-rays detected from this AGN is too low. For NGC 1851 and NGC 6723, the nearest AGNs are [VV96] J050920.2-410249 and UVQS J190411.10-341010.7, their distances away from are NGC 1851 and NGC 6723 are $\sim1°.4$ and $2°.6$, respectively. Their offsets are too larger. These cases increase the probability that the gamma-ray emissions detected here come from the three GCs.

In the significantly detected GCs, their SED showed a shape of power-law with a super exponential cutoff, e.g., 47 Tuc, Terzan 5, and so on (Abdo et al. 2009, 2010a; de Menezes et al. 2019). As listed in Table 2, two spectral models are employed in our data reduction. No obvious difference is detected for the TS values of two spectral models, this result may be caused by

---

[10] https://simbad.u-strasbg.fr/simbad/

that the relatively little events from these GCs cannot to constrain their spectral shape better. A main difference between the three GCs detected here and those reported in the previous literature is that their distances are much larger than those listed in Abdollahi et al. (2020), Ballet et al. (2020).

The number of MSPs in each GC reported here was estimated in our analysis. From Table 2, the estimated MSP number in NGC 1851 is roughly consistent with the observed one in error range, but no radio and/or X-ray pulsars are detected in NGC 6715 and NGC 6723. In fact, the estimated number of MSPs in each GC is much greater than the detected number for the most of gamma-ray GCs (see Table 3). For example, Terzan 5, it has been detected to have 39 MSPs so far, but the estimated number of MSPs given by Abdo et al. (2010a) is ~ 180, our result is 317 ± 123. Up to now, about 230 MSPs have been identified in 36 GCs,[11] however about 2600 -4700 MSPs are predicted in Galactic GCs that are observable in gamma-rays (Abdo et al. 2010a). In the future more pulsars will be detected by radio and/or X-ray telescopes (Nan et al. 2011; Li & Pan 2016; Ridolfi et al. 2019).

Generally GCs are located at the distances from several to more than a hundred kpc (the nearest NGC 6121 at 2.2 kpc and the farthest AM 1 at 123.3 kpc). It is more distant than most gamma-ray pulsars observed in the Milky Way. A possible reason is that the gamma-ray flux of a single MSP is too weak to be detected at several kpc, but many MSPs in a GC can be responsible to the observed gamma-rays. In this scenario, the observed gamma-ray emissions from GCs may be associated with MSPs inside themselves, they may come from pulsed synchro-curvature mechanism arising near the polar cap and/or in outer magnetospheric gaps (Zhang & Cheng 1997, 2003) or inverse Compton scattering between the relativistic particles (electrons/positrons) in the pulsar winds and the soft photons around the Galactic plane background (Bednarek & Sitarek 2007; Cheng et al. 2010).

It should be pointed out that there are other possible origins of gamma-rays from GCs, such as pulsar binary systems and/ or DM.

It is well-known that the most of MSPs hosted in GCs are detected in binary systems, including LMXBs and binary MSPs (the redback or black widow systems). For example, GC 47 Tucanae hosts 27 MSPs within it, 10 of them are isolated, 17 MSPs are the part of pulsar binary systems with periods range spanning from approximately 0.07 up to 11 days, six of them belong to black widow systems (including four eclipsing black widows), and three are eclipsing redback systems. A gamma-ray periodic modulation with a period of ~ 18.4 hr (~ 0.77 day) is detected by Zhang et al. (2020). The period is much longer than that spin period found in MSPs hosted in GCs, so this periodic modulation signal detected in 47 Tucanae cannot be the spin period of pulsar and it is indeed well within the range

of periods of pulsar binary systems. This may claim that this periodic modulation is induced by the possible presence of more MSP binaries in 47 Tucanae (Zhang et al. 2020), but not detected now. Several binary MSPs are also identified as gamma-ray emitters (Guillemot et al. 2012; Wu et al. 2012; Xing & Wang 2015), including black widow and/or redback binary systems, they also show orbital modulations in gamma-rays produced by inverse Compton scattering (Cheng et al. 2006; Tam et al. 2011a; Ng et al. 2018; Clark et al. 2021) or synchrotron emission from particles accelerated along the shock front, which may be a scenario to explain the gamma-ray emitting from GCs.

Another scenario is that Galactic GCs are thought to form in the cosmological context with adiabatic contraction process (Peebles 1984; Bertone & Fairbairn 2008; Wood et al. 2008; Zaharijaš 2008; Baumgardt et al. 2009; Lane et al. 2010; McCullough & Fairbairn 2010; Conroy et al. 2011; Bertoni et al. 2015; Amaro-Seoane et al. 2016; Brown et al. 2018; Dasgupta et al. 2019), this makes them potential targets for the indirect detection of DM. But the three GCs are relatively weaker compared with the significant GCs, they are not suitable for the studying of whether the gamma-rays arise from DM in GCs. We do not discuss detailedly their gamma-ray origins here, since these topics are beyond the scope of this work. Some new gamma-ray missions, such as Very Large Area gamma-ray Space Telescope (VLAST), may shed some light for the origins of gamma-rays from GCs (Fan et al. 2022).

Acknowledgments

References

Abdo, A. A., Ackermann, M., Ajello, M., et al. 2009, Sci, 325, 845
Abdo, A. A., Ackermann, M., Ajello, M., et al. 2010a, A&A, 524, A75
Abdo, A. A., Ackermann, M., Ajello, M., et al. 2010b, ApJS, 188, 405
Abdollahi, S., Acero, F., Ackermann, M., et al. 2020, ApJS, 247, 33
Abramowski, A., Acero, F., Aharonian, F., et al. 2011, ApJ, 735, 12
Acero, F., Ackermann, M., Ajello, M., et al. 2015, ApJS, 218, 23
Alpar, M. A., Cheng, A. F., Ruderman, M. A., & Shaham, J. 1982, Natur, 300, 728
Amaro-Seoane, P., Casanellas, J., Schödel, R., Davidson, E., & Cuadra, J. 2016, MNRAS, 459, 695
Atwood, W. B., Abdo, A. A., Ackermann, M., et al. 2009, ApJ, 697, 1071
Ballet, J., Burnett, T. H., Digel, S. W., & Lott, B. 2020, arXiv:2005.11208
Baumgardt, H., Côté, P., Hilker, M., et al. 2009, MNRAS, 396, 2051
Bednarek, W., & Sitarek, J. 2007, MNRAS, 377, 920
Bertone, G., & Fairbairn, M. 2008, PhRvD, 77, 043515
Bertoni, B., Hooper, D., & Linden, T. 2015, JCAP, 2015, 035
Booth, R. S., & Jonas, J. L. 2012, AfrSk, 16, 101

---

[11] http://www.naic.edu/~pfreire/GCpsr.html

Brown, A. M., Lacroix, T., Lloyd, S., Bœhm, C., & Chadwick, P. 2018, PhRvD, 98, 041301

Cheng, K. S., Chernyshov, D. O., Dogiel, V. A., Hui, C. Y., & Kong, A. K. H. 2010, ApJ, 723, 1219

Cheng, K. S., Ho, C., & Ruderman, M. 1986, ApJ, 300, 500

Cheng, K. S., Taam, R. E., & Wang, W. 2006, ApJ, 641, 427

Clark, C. J., Nieder, L., Voisin, G., et al. 2021, MNRAS, 502, 915

Clark, G. W. 1975, ApJL, 199, L143

Conroy, C., Loeb, A., & Spergel, D. N. 2011, ApJ, 741, 72

Dasgupta, B., Gupta, A., & Ray, A. 2019, JCAP, 2019, 018

de Menezes, R., Cafardo, F., & Nemmen, R. 2019, MNRAS, 486, 851

Djorgovski, S. 1993, in ASP Conf. Ser. 50, Structure and Dynamics of Globular Clusters, ed. S. G. Djorgovski & G. Meylan (San Francisco, CA: ASP), 373

Eger, P., & Domainko, W. 2012, A&A, 540, A17

Fan, Y. Z., Chang, J., Guo, J. H., et al. 2022, AcASn, 63, 27

Feng, L., Yuan, Q., Yin, P.-F., Bi, X.-J., & Li, M. 2012, JCAP, 2012, 030

Fortes, E. C., Miranda, O. D., Stecker, F. W., & Wuensche, C. A. 2020, JCAP, 2020, 010

Freire, P. C. C., Abdo, A. A., Ajello, M., et al. 2011, Sci, 334, 1107

Gendre, B., Barret, D., & Webb, N. 2003, A&A, 403, L11

Grindlay, J. E., Heinke, C., Edmonds, P. D., & Murray, S. S. 2001, Sci, 292, 2290

Guillemot, L., Johnson, T. J., Venter, C., et al. 2012, ApJ, 744, 33

Harding, A. K., Usov, V. V., & Muslimov, A. G. 2005, ApJ, 622, 531

Harris, W. E. 1996, AJ, 112, 1487

Heinke, C. O., Grindlay, J. E., Edmonds, P. D., et al. 2005, ApJ, 625, 796

Henleywillis, S., Cool, A. M., Haggard, D., et al. 2018, MNRAS, 479, 2834

Hui, C. Y., Cheng, K. S., Wang, Y., et al. 2011, ApJ, 726, 100

Ibata, R., Bellazzini, M., Chapman, S. C., et al. 2009, ApJL, 699, L169

Johnson, T. J., Guillemot, L., Kerr, M., et al. 2013, ApJ, 778, 106

Kong, A. K. H., Hui, C. Y., & Cheng, K. S. 2010, ApJL, 712, L36

Lane, R. R., Kiss, L. L., Lewis, G. F., et al. 2010, MNRAS, 406, 2732

Li, D., & Pan, Z. 2016, RaSc, 51, 1060

Liu, Q. Z., van Paradijs, J., & van den Heuvel, E. P. J. 2007, A&A, 469, 807

Lloyd, S. J., Chadwick, P. M., & Brown, A. M. 2018, MNRAS, 480, 4782

MAGIC Collaboration, Acciari, V. A., Ansoldi, S., et al. 2019, MNRAS, 484, 2876

Manchester, R. N., Hobbs, G. B., Teoh, A., & Hobbs, M. 2005, AJ, 129, 1993

McCullough, M., & Fairbairn, M. 2010, PhRvD, 81, 083520

Nan, R., Li, D., Jin, C., et al. 2011, IJMPD, 20, 989

Ndiyavala, H., Venter, C., Johnson, T. J., et al. 2019, ApJ, 880, 53

Ng, C. W., Takata, J., Strader, J., Li, K. L., & Cheng, K. S. 2018, ApJ, 867, 90

Nolan, P. L., Abdo, A. A., Ackermann, M., et al. 2012, ApJS, 199, 31

Oh, K., Hui, C. Y., Li, K. L., & Kong, A. K. H. 2020, MNRAS, 498, 292

Peebles, P. J. E. 1984, ApJ, 277, 470

Ridolfi, A., Freire, P. C. C., Gupta, Y., & Ransom, S. M. 2019, MNRAS, 490, 3860

Song, D., Macias, O., Horiuchi, S., Crocker, R. M., & Nataf, D. M. 2021, MNRAS, 507, 5161

Tam, P. H. T., Huang, R. H. H., Takata, J., et al. 2011a, ApJL, 736, L10

Tam, P.-H. T., Hui, C. Y., & Kong, A. K. H. 2016, JASS, 33, 1

Tam, P. H. T., Kong, A. K. H., Hui, C. Y., et al. 2011b, ApJ, 729, 90

Venter, C., & de Jager, O. C. 2008, ApJL, 680, L125

Wei, D. M., Cheng, K. S., & Lu, T. 1996, ApJ, 468, 207

Wood, M., Blaylock, G., Bradbury, S. M., et al. 2008, ApJ, 678, 594

Wu, E. M. H., Takata, J., Cheng, K. S., et al. 2012, ApJ, 761, 181

Wu, J. H. K., Hui, C. Y., Wu, E. M. H., et al. 2013, ApJL, 765, L47

Wu, W., Wang, Z., Xing, Y., & Zhang, P. 2022, ApJ, 927, 117

Xing, Y., & Wang, Z. 2015, ApJL, 804, L33

Yuan, M., Zheng, J., Zhang, P., & Zhang, L. 2022, RAA, 22, 055019

Zaharijaš, G. 2008, PhRvD, 78, 027301

Zajczyk, A., Bednarek, W., & Rudak, B. 2013, MNRAS, 432, 3462

Zhang, L., & Cheng, K. S. 1997, ApJ, 487, 370

Zhang, L., & Cheng, K. S. 2003, A&A, 398, 639

Zhang, P., Xing, Y., & Wang, Z. 2022, ApJL, 935, L36

Zhang, P. F., Xin, Y. L., Fu, L., et al. 2016, MNRAS, 459, 99

Zhang, P.-F., Zhou, J.-N., Yan, D.-H., et al. 2020, ApJL, 904, L29

Zhao, Y., Heinke, C. O., Cohn, H. N., et al. 2020, MNRAS, 499, 3338

Zhou, J. N., Zhang, P. F., Huang, X. Y., et al. 2015, MNRAS, 448, 3215